IEEE Access
Multidisciplinary | Rapid Review | Open Access Journal

Received February 16, 2020, accepted March 3, 2020, date of publication March 9, 2020, date of current version March 24, 2020.

Digital Object Identifier 10.1109/ACCESS.2020.2979504

Optimal Deployment of Antenna for Field Coverage in Coal Mine Tunnels

YU HUO[1], (Member, IEEE), LEI ZHAO[2], (Senior Member, IEEE), QINGSONG HU[1,2], ENJIE DING[1], XIAOHU ZHAO[1], AND ZHI SUN[3], (Member, IEEE)

[1]National Joint Engineering Laboratory of Internet Applied Technology of Mines, China University of Mining and Technology, Xuzhou 221116, China
[2]School of Information and Control Engineering, China University of Mining and Technology, Xuzhou 221116, China
[3]Department of Electrical Engineering, State University of New York at Buffalo, Buffalo, NY 14260, USA

Corresponding authors: Lei Zhao (leizhao@cumt.edu.cn) and Xiaohu Zhao (xiaohuzhao@126.com)

This work was supported in part by the National Key Research and Development Project under Grant 2017YFC0804404, in part by the National Natural Science Foundation of China under Grant 61841114, Grant 61901475, Grant 61771226, and Grant 51874299, in part by the Natural Science Foundation of Jiangsu Province under Grant BK20160264, and in part by the Fundamental Research Funds for the Central Universities under Grant 2019CXNL07.

ABSTRACT A deployment strategy for antennas is proposed to enhance the field coverage of wireless devices in underground coal mines, which uses the multimodal approach. Based on the attenuation coefficient of each mode, the propagation loss of the vertically polarized modes with $n = 1$, 2, and 3 and that of the horizontally polarized modes with $m = 1$, 2, and 3 are less. For the signal propagation in the near-field region of the source, these modes play significant role. According to the coupling of the antenna to the modes, the significant modes can be effectively excited by mounting horizontally polarized antenna on the ceiling or the vertically polarized antenna on the sidewall. For the signal propagation in the far-field region, the (1, 1) mode is significant, and the horizontally polarized excitation is preferred due to smaller attenuation. By comparing the total coupling efficiency of the antenna-radiated power, stronger excitation power can be obtained by mounting the antenna near the center of the ceiling or that of the sidewall. The field strength in the near-field and far-field region coverage can be maximized by optimizing the antenna polarization and position. For verification, a grid-based test system was designed and a series of measurements inside an underground coal mine tunnel were conducted. The measured results have a good agreement with the theoretical ones. In addition, the EM interference caused by the infrastructure in real mines on the signal received by the antennas at different positions was also measured and compared. Results show that the influences of cables with long-term stable loads, such as power cables and communication cables, can be neglected.

INDEX TERMS Antenna deployment, field coverage, underground mines, wireless networks.

I. INTRODUCTION

Field coverage with higher intensity conduces to less power consumption and longer battery life of the wireless devices. It also helps to reduce data retransmissions and enhance link reliability. However, the radio signals in coal mines do not propagate well due to the bounding of the tunnel walls [1]–[5].

The radio field coverage in underground mines can be enhanced by antenna polarization and position [4]–[7]. In previous studies [4]–[6], the field distributions in terms of different antenna positions were discussed by geometrical optical approach. In [7], the effects of antenna position and polarization on ultra-wideband (UWB) radio propagation in mines were studied by measurements. However, the reported antenna deployment strategies have not considered the difference in coverage requirements for different wireless devices. Most existing UWB-based sensor network proposals were intended to operate in the near-field region of the source. Nevertheless, other sensor network proposals, which were based on wireless fidelity (WiFi), ZigBee and long range (LoRa), were intended to operate in the far-field region of the source. Great differences were observed in the mechanism and characteristics of the signal propagation between these two regions [8]–[10]. Therefore, the effects of the antenna position and polarization on wireless path loss in these two

The associate editor coordinating the review of this manuscript and approving it for publication was Chuan Huang.

regions were different. A specific deployment strategy of the antenna is necessary for a wireless proposal with the actual coverage requirement.

In this paper, a new deployment strategy was proposed based on multimode theory [11]–[15]. The field propagation characteristics in the near-field and far-field region of the source in underground mines were investigated, respectively. A grid-based test system was designed to validate the proposed method. Good agreements were found between the theoretical and measured results. In addition, the limitations of the spatiotemporal EM interference caused by infrastructure in real mines on the antenna deployment strategy were also discussed; through a series of measurements. This study mainly addressed the wireless coverage of the fixed nodes, with the antennas generally mounted near the walls.

The major contributions of this study were as follows:

1) Infer the significant modes that play a key role in signal propagation in the near-field and far-field regions of the source.
2) Deduce the fractions of the antenna-radiated power coupled into each mode and into the entire field, respectively.
3) Understand the influence mechanism of the antenna on the field fading; and then propose the optimal antenna polarization and position for the field coverage in the near-field and far-field region.

The remainder of this manuscript is organized as follows. Section II describes the coupling relationship between the antenna and the characteristic modes, and provides a theoretical optimal deployment method for the antenna. Section III presents the tunnel environment, and the measurement system and procedure. Section IV presents a comparison of the results of measurement and simulation. Section V provides the conclusion.

II. METHODOLOGY

A. PROPAGATION CHARACTERISTICS OF THE TUNNEL FIELD

The multimodal approach [11]–[15] for rectangular tunnels is a very representative method used to simplify the solution of the EM field in tunnels with other transversal shapes, such as arched tunnels [16]–[19]. In a rectangular tunnel, set a Cartesian coordinate system with its origin located at the center of the tunnel. x, y, and z axes are along the width, height, and length of the tunnel, respectively. With reference to the quantities listed in Table 1, the $(\vec{\mathrm{E}}, \vec{\mathrm{H}})$ field can be expressed as the superimposition of multiple horizontally/vertically polarized modes with indexes (m, n) [11], [14], [15]:

$$\vec{\mathrm{E}} = \sum_m \sum_n \vec{\mathrm{E}}_{mn} = \sum_m \sum_n E_{0mn} \cdot \vec{\mathrm{e}}_{mn} \cdot \exp\left[-\gamma_{mn}(z - z_0)\right] \tag{1}$$

$$\vec{\mathrm{H}} = \sum_m \sum_n \vec{\mathrm{H}}_{mn} = \sum_m \sum_n E_{0mn} \cdot \vec{\mathrm{h}}_{mn} \cdot \exp\left[-\gamma_{mn}(z - z_0)\right] \tag{2}$$

TABLE 1. List of quantities used in EM field description.

Symbol	Quantity
w	width of the rectangular tunnel
h	height of the rectangular tunnel
(x_0, y_0, z_0)	coordinate of the transmitting antenna
(x, y, z)	coordinate of the receiving antenna
m, n	order of the waveguide mode
$\vec{\mathrm{E}}$	electric field
$\vec{\mathrm{H}}$	magnetic field
$\vec{\mathrm{E}}_{mn}$	electric field along the (m, n) mode
$\vec{\mathrm{H}}_{mn}$	magnetic field along the (m, n) mode
E_{0mn}	intensity of the (m, n) mode excited by the antenna
$\vec{\mathrm{e}}_{mn}$	mode function of $\vec{\mathrm{E}}_{mn}$
$\vec{\mathrm{h}}_{mn}$	mode function of $\vec{\mathrm{H}}_{mn}$
γ_{mn}	mode propagation constant of the (m, n) mode along z axis
α_{mn}	attenuation coefficient of the (m, n) mode
β_{mn}	phase-shift coefficient of the (m, n) mode
λ	wavelength
M	total number of modes in the tunnel
ϕ_x	for vertical polarization, ϕ_x=0 if m is odd and ϕ_x=$\pi/2$ if m is even.
ϕ_y	for vertical polarization, ϕ_y=$\pi/2$ if n is odd and ϕ_y=0 if n is even.
Z_0	EM wave impedance in the air.
k_0	wave number in the tunnel space
$K1$	relative permittivity of the tunnel sidewall
$K2$	relative permittivity of the tunnel ceiling/floor

where the restrictions of m and n are given by [20]

$$1 \le |m| \le m_{\lim} = \lfloor 2w/\lambda \rfloor \tag{3}$$

$$1 \le |n| \le n_{\lim} = \lfloor 2h/\lambda \rfloor \tag{4}$$

The modes are transmitted symmetrically along the forward and backward directions of the antenna in the tunnel [21], [22]. When only one direction is considered, the total number of modes in the tunnel is $M = (2 \cdot 2w/\lambda) \cdot (2 \cdot 2h/\lambda) = 16wh/\lambda^2$.

For the vertically polarized field, the (m, n) mode can be characterized by the following approximated expressions [20] (similar formulas hold for the horizontally polarized field)

$$\vec{\mathrm{e}}_{mn} \approx \hat{i}_y \cdot e_{m,n} = \hat{i}_y \cdot \cos\left(\frac{m\pi}{w}x + \phi_x\right) \sin\left(\frac{n\pi}{h}y + \phi_y\right) \tag{5}$$

$$\vec{\mathrm{h}}_{mn} \approx \hat{i}_x \cdot \frac{e_{m,n}}{Z_0} \tag{6}$$

$$\alpha_{mn} = \frac{2m^2\pi^2}{k_0^2 w^3} Re \frac{1}{\sqrt{K1 - 1}} + \frac{2n^2\pi^2}{k_0^2 h^3} \mathrm{Re} \frac{K2}{\sqrt{K2 - 1}} \tag{7}$$

$$\beta_{mn} = \sqrt{k_0^2 - \left(\frac{m\pi}{w}\right)^2 - \left(\frac{n\pi}{h}\right)^2} \tag{8}$$

where $Z_0 = 120\pi\,\Omega$, and $k_0 = 2\pi/\lambda$. $K1$ and $K2$ are often assumed as $K1 = K2$ [14], [15], [21], [22].

According to the propagation characteristics of the wireless signal in mine tunnels, the variation of the EM field in the tunnel is mainly characterized by the first few modes with less attenuation [14], [15]. These modes are defined as significant modes [8]–[10], [13]. When the receiver is close to the transmitter, the difference in attenuation among modes is small. Hence, multiple significant modes play critical roles in the coverage field. When the receiver is far away from the transmitter, the difference among modes is large. With the rapid attenuation of the higher-order mode, the dominant role is gradually concentrated on the least-attenuated mode. The multimode zone is called the near-field region, while the other is called the far-field region [8]–[10], [13]. The breakpoint between these two regions can be determined by $\max\left(w^2/\lambda, h^2/\lambda\right)$ [8].

B. MODES WITH LESS PROPAGATION LOSS

For a given condition of excitation, the total attenuation of L_{mn} the (m, n) mode is given by

$$L_{mn} = Cop_{mn} + MAF_{mn} \tag{9}$$

where Cop_{mn} represents the loss due to the coupling of the radiated power of the antenna to the (m, n) mode (deduced in Section IIC). MAF_{mn} represents the loss due to the propagation of the (m, n) mode. The significant modes with smaller Cop_{mn} and smaller MAF_{mn} are helpful in coverage. This section first discusses MAF_{mn}.

1) FOR NEAR-FIELD REGION COVERAGE

For a straight and smooth tunnel [15],

$$MAF_{mn} = -20\log_{10}\left[e^{-\alpha_{mn}(z-z_0)}\right] = 8.686\alpha_{mn}\,(z - z_0) \tag{10}$$

Substituting α_{mn} from (7) into (10), and considering the general assumption of $K1$ and $K2$, the MAF_{mn} for vertical polarization becomes

$$MAF_{mn} = 8.686z\frac{2\pi^2}{k_0^2}\mathrm{Re}\frac{1}{\sqrt{K1-1}}\left(\frac{m^2}{w^3} + \frac{n^2K1}{h^3}\right) \tag{11}$$

According to (11), MAF_{mn} increases with the value of m and n. When $K1/h^3 > 1/w^3$, the growth of MAF_{mn} with n is faster than that with m. This condition is satisfactory for most mines, because most of the coal mine tunnels have a larger width than height. Therefore, the vertically polarized modes with less propagation loss in the near-field region are mainly the modes with a lower order of n, such as $n = 1$, 2, and 3. As the structure of the rectangular roadway is symmetrical, the horizontally polarized modes with less propagation loss in the near-field region are mainly the modes with a lower order of m, such as $m = 1$, 2, and 3.

2) FOR FAR-FIELD REGION COVERAGE

The propagation loss of the fundamental mode, namely (1, 1) mode, is the least, according to (11).

C. EFFECTIVE EXCITED POSITION FOR MODES

With reference to an antenna with the maximum current I_0 and the current density $\vec{\mathrm{J}}$ in the region V, E_{0mn} is given by

$$E_{0mn} = \frac{1}{\sqrt{M}}Z_0\iiint_V (\boldsymbol{i}_z \times I_0\vec{\mathrm{J}})\cdot\left(\vec{\mathrm{h}}_{mn}\cdot\exp\left[-\gamma_{mn}\,(z-z_0)\right]\right)dV \tag{12}$$

If the antenna size is much smaller than the cross section of the tunnel, E_{0mn} is simplified to,

$$E_{0mn} = \frac{I_0Z_0\iiint_V \vec{\mathrm{J}}dV}{\sqrt{M}}\cos\left(\frac{m\pi}{w}x_0 + \phi_x\right)\sin\left(\frac{n\pi}{h}y_0 + \phi_y\right) \tag{13}$$

The antenna-radiated power coupled into the (m, n) mode propagating into one tunnel direction is

$$\begin{aligned} P_{0mn} &= \frac{|E_{0mn}|^2}{Z_0} \\ &\approx \frac{I_0^2Z_0\left(\iiint_V \vec{\mathrm{J}}dV\right)^2}{M}\cos^2\left(\frac{m\pi}{w}x_0+\phi_x\right)\sin^2\left(\frac{n\pi}{h}y_0+\phi_y\right) \end{aligned} \tag{14}$$

The power radiated by the antenna in one direction is $P_{antenna} = I_0^2R_{in}/2$, where R_{in} is the radiation resistance of the antenna. Then, the fraction η_{mn} of the radiated power coupled into the (m, n) mode is

$$\begin{aligned} \eta_{mn} &= \frac{P_{0mn}}{P_{antenna}} \\ &= \frac{2Z_0\left(\iiint_V \vec{\mathrm{J}}dV\right)^2}{MR_{in}}\cos^2\left(\frac{m\pi}{w}x_0+\phi_x\right)\sin^2\left(\frac{n\pi}{h}y_0+\phi_y\right) \end{aligned} \tag{15}$$

The loss Cop_{mn} in the (m, n) mode in dB is,

$$Cop_{mn} = -10\log_{10}(\eta_{mn}) \tag{16}$$

1) FOR NEAR-FIELD REGION COVERAGE

From (15), the position of maximum coupling of the transmitting antenna for the (m, n) mode is,

$$\begin{cases} x_0 = \pm\dfrac{kw}{m}, & \text{if } m \text{ is odd} \\ x_0 = \pm\dfrac{(2k+1)\,w}{2m}, & \text{if } m \text{ is even} \end{cases} \tag{17}$$

$$\begin{cases} y_0 = \pm\dfrac{kh}{n}, & \text{if } n \text{ is odd} \\ y_0 = \pm\dfrac{(2k+1)\,h}{2n}, & \text{if } n \text{ is even} \end{cases} \tag{18}$$

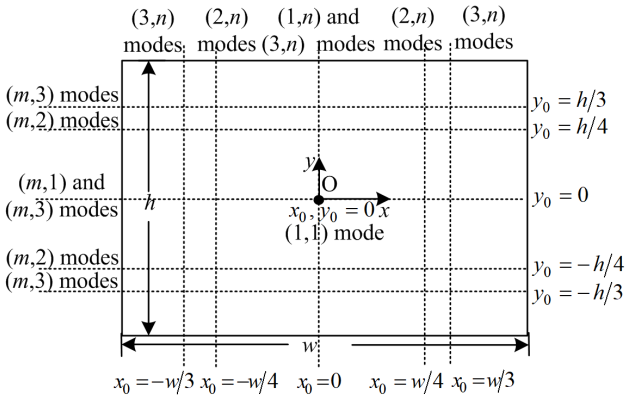

FIGURE 1. Effective excited positions of the antenna for modes with less propagation loss.

where k is an integer. By similar derivation, (17) and (18) are also suitable for horizontally polarized waves. Substituting the first modes into (17) and (18), the corresponding most effective coupling positions of the antenna were obtained and are shown in Fig.1. Cop_{m1} and Cop_{m3} are the least when the antenna is located at $y_0 = 0$, and Cop_{m2} is the least when the antenna is located at $y_0 = \pm h/4$. Cop_{m3} is also the least when the antenna is located at $y_0 = \pm h/3$. As deduced in Section IIB, the MAF_{mn} values of $n = 1$, 2 and 3 modes are the least for the vertically polarized field. Consequently, mounting the vertically polarized antenna on these locations, namely the sidewalls of the tunnel, $n = 1$, 2 and 3 modes become the significant modes and result in less propagation loss for field coverage in the near-field region. Similarly, for the horizontally polarized antenna, the mounting location with less propagation loss in the near-field region is the ceiling of the tunnel.

By comparing MAF_{mn} for the horizontally and the vertically polarized modes [20], it can be deduced that the vertical polarization can obtain less propagation loss when $(h/w)^3 > (n/m)^2$. From Fig.1, when the antenna is near the sidewalls, the most excited modes are those with a lower order of n but a higher order of m (m is usually larger than 3, but n can be the least). In this case, $(h/w)^3 > (n/m)^2$ is satisfactory for most mines, so horizontal polarization can easily lead to greater field fading. Similarly, when the antenna is near the ceiling, vertical polarization tends to provide greater field fading.

2) FOR FAR-FIELD REGION COVERAGE

According to (15) and (16), Cop_{mn} is unrelated to the propagation distance from the transmitter, while MAF_{mn} increases linearly with it. When the distance is long enough, the value of Cop_{mn} is too small compared with that of MAF_{mn}. Hence, the difference in Cop_{mn} among modes can be negligible, while the difference in MAF_{mn} is gradually significant. The (1, 1) mode has the least propagation loss. Hence, it is the most significant mode in the far-field region. By comparing MAF_{11}, it can be seen that the propagation loss of the horizontally polarized (1, 1) mode is lower than that of the vertically polarized (1, 1) mode if the tunnel have a larger width than height, so horizontal polarization has less propagation loss in the far-field region. In Fig.1, the maximum coupling position for (1, 1) mode is the center of the tunnel. However, it is the optimal position only for mobile devices in underground mines.

D. ANTENNA COUPLING EFFICIENCY

The higher coupling efficiency of the antenna can provide greater excitation power of the signal. It rather helps to increase the field strength and range of wireless coverage.

1) FOR NEAR-FIELD REGION COVERAGE

Considering the contribution of multiple significant modes for the near-field propagation, the total coupled power P_0 of the antenna in one tunnel direction is [11]–[15], [21],

$$P_0 = \frac{\left|\sum_m \sum_n E_{0mn}\right|^2}{Z_0} \tag{19}$$

Substituting (13) into (19), P_0 is given by

$$P_0 = \frac{1}{M} I_0^2 Z_0 \left|\iiint_V \vec{\mathrm{J}} dV\right|^2 \left|\sum_m \cos\left(\frac{m\pi}{w} x_0 + \phi_x\right)\right|^2 \cdot \left|\sum_n \sin\left(\frac{n\pi}{h} y_0 + \phi_y\right)\right|^2 \tag{20}$$

The overall coupling efficiency η is the overall fraction of the radiated power that is coupled into the multiple modes. η is given by

$$\eta = \frac{P_0}{P_{antenna}} = \delta_V \left|\sum_n \sin\left(\frac{n\pi}{h} y_0 + \phi_y\right)\right|^2 \tag{21}$$

in which $\delta_V = \frac{2Z_0}{MR_{in}} \left|\iiint_V \vec{\mathrm{J}} dV\right|^2 \left|\sum_m \cos\left(\frac{m\pi}{w} x_0 + \phi_x\right)\right|^2$.

The total coupling loss Cop in dB is obtained by

$$Cop = -10 \log_{10}(\eta) \tag{22}$$

Similar formulas hold for η and Cop excited by the horizontally polarized antenna.

Table 2 provides the overall coupling efficiency of the antenna for the effective excited positions discussed in Sections IIC. In Table 2, δ_H is a constant with a similar expression as δ_V. Table 2 shows that the vertically polarized antenna can provide higher coupling efficiency when it is located at the center of the sidewall, while the horizontally polarized antenna can provide higher coupling efficiency when it is located at the center of the ceiling. These antenna deployments are optimal for the near-field region coverage.

Besides, the vertically/horizontally polarized antenna can result in the lowest coupling efficiency when it is located at $y_0 = \pm h/3$ or $x_0 = \pm w/3$, which is close to the corner of the tunnel cross section.

TABLE 2. Coupling efficiency for vertically polarized antenna at effective excited positions.

Vertical polarization			
Location	Antenna at $y_0 = 0$	Antenna at $y_0 = \pm h/4$	Antenna at $y_0 = \pm h/3$
Coupling efficiency	$4\delta_V$	δ_V	$0.134\delta_V$
Horizontal polarization			
Location	Antenna at $x_0 = 0$	Antenna at $x_0 = \pm w/4$	Antenna at $x_0 = \pm w/3$
Coupling efficiency	$4\delta_H$	δ_H	$0.134\delta_H$

2) FOR FAR-FIELD REGION COVERAGE

In the far-field region, the importance of the higher order modes is greatly reduced due to the rapid attenuation, and the (1, 1) mode is dominant. Fig.2 shows the coupling efficiency between the (1, 1) mode and the antenna installed at all locations with respect to the tunnel cross section. The value is normalized by the maximum coupling efficiency. The results for vertical and horizontal polarization are the same. From Fig.2, it is obvious that the (1, 1) mode can get stronger coupling power of the antenna when it is located at the center of the sidewall or that of the ceiling. Therefore, these mounting positions are optimal for the far field region coverage. Fig.2 also shows that the antenna mounted at the corner of the tunnel cross section results in the minimum coupling efficiency, hence provides the weakest coverage.

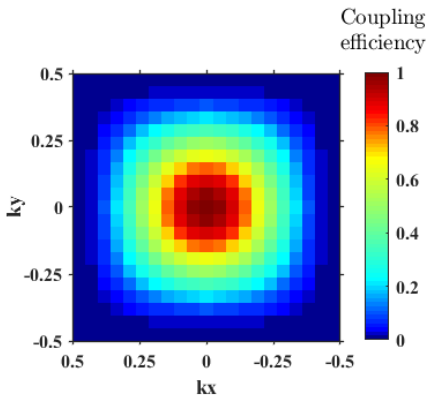

FIGURE 2. Normalized coupling efficiency for all the antenna locations with respect to the tunnel cross section. The antenna location is $x_0 = kx \cdot w$ and $y_0 = ky \cdot h$, where the range of kx and ky is -0.5–0.5.

The deduction and discussion in this section are satisfactory for tunnels with a larger width than height. In a rectangular tunnel, the horizontally polarized and the vertically polarized fields are opposite [10], [14], [15], [22]. Consequently, if the width of the tunnel is shorter than its height, the optimal deployment strategy should be reversed. However, in perfectly square cross-sectioned galleries, no difference is found in field strength between the horizontally polarized antenna on the ceiling and the vertically polarized antenna on the side wall, and also no difference between the horizontally polarized antenna on the side wall and the vertically polarized antenna on the ceiling.

III. EXPERIMENTAL SETUP AND PROCEDURE

A measurement campaign was carried out inside an underground tunnel located at the Xinglongzhuang Coal Mine, Shandong Province, China, to verify the theory.

A. PHYSICAL ENVIRONMENT

Fig.3 shows the inside view of the measurement tunnel, which was an arched service tunnel. The radius of the transverse section of the arched tunnel was about 2.69 m, the width of the flat base was about 5.12 m, and the maximum height was about 3.56 m. The testing area of the tunnel was a relative straight line section with a length of 200 m. The roadway walls were made of rock. Uneven deformation occurred in the sidewalls and the ceiling. The pipes, power cables, and communication cables were arranged on the sidewalls. An overhead cable for narrow-gauge electromechanical vehicles was suspended at the center of the roof.

FIGURE 3. Inside view of the coal mine tunnel with the measurement system.

B. EXPERIMENT SETUP

An experimental system based on the grid concept was designed, which could be used to conduct multiple simultaneous sender–receiver tests [23]. The diagram of the experimental system is shown in Fig.4. AS32-TTL-1W LoRa nodes developed by Chengdu Ashining Technology Company, Ltd. were chosen to perform the measurements. The nodes could provide Received Signal Strength Indication (RSSI). The transmitting power was 21 dBm. The frequency used was 433 MHz. The receiving sensitivity of the node was –130 dBm. The antenna of the node was linearly polarized.

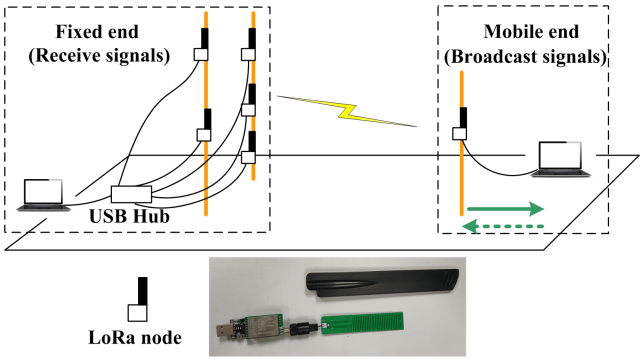

FIGURE 4. Diagram of the experimental system.

When it was placed parallel to the floor but perpendicular to a side wall, it was horizontally polarized [10], [18]. On reverse alignment, it was vertically polarized. The mobile end of the grid-based setup used a single node to broadcast the test signals, while the fixed end used multiple nodes to simultaneously receive signals. Each node was connected to the computer via Universal Serial Bus (USB) cables to define the configuration of the sending data or to download the received data. The statistical analysis included the calculation of the mean and standard deviation (SD) of RSS, and the packet loss rate (PLR) for each transceiving period. The experimental software was self-developed by Eclipse.

The coverage field of the antenna was measured at five positions, which were denoted as center (C), ceiling center (CC), corner (CO), sidewall center (WC), and the widest part of the sidewall (WW). At the mobile end, the antenna was placed at the C position. Fig.5 shows the positions of the antennas, which refers to the position of the center of the antenna. After each group of packet test, the transmitting node moved backward along the track by 1.40 m distance.

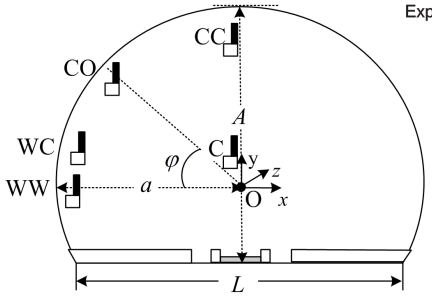

Experimental Coordinates of Antenna

The fixed end	
C	(-0.28,0.89,0)
CC	(-0.04,2.40,0)
CO	(-1.62,1.90,0)
WC	(-2.30,0.90,0)
WW	(-2.45, 0.02,0)
The mobile end	
C	(0, 0.94, z)

a=2.70m, A=3.63m, L=5.04m, and $\varphi=\pi/4$ rad

FIGURE 5. Cross section of the arched tunnel with antenna positions.

C. EXPERIMENT PROCEDURE

In the experiments, a set of LoRa nodes were firstly compared and calibrated to reduce the differences in the sensitivities of their RSSI. The configuration of the sending data during one sending period was defined as follows:

The total number of packets was 300, with each packet containing 40 bytes, and the delay of each packet was 600 ms. Under such conditions, the measured data in the test area showed that RSSI average varied at most ±1 dBm from the mean value for the set of nodes, when PLR of each node was less than 30% and SD of RSSI of each node in one experiment was less than 2.8 dBm. PLR and SD were used to judge the effectiveness of the received signal during one test. The duration of one period was about 3 min. The average RSSI was recorded by calculation over 300 packets 2 times.

IV. EXPERIMENTAL RESULTS AND DISCUSSION

Fig.6 shows the simulation parameters. Fig.7 and Fig.8 show the measured and simulated Received Signal Strength (RSS) of the vertically polarized (denoted by VV) and the horizontally polarized (denoted by HH) antenna at different locations in the tunnel, respectively. Using the method in [17], [18], the arched tunnel for the experiments was equivalently surrogated by a rectangular tunnel with 5.10 m width and 3.43 m height. The location of WW in the arched tunnel was moved to the center of the sidewall to adjust to the surrogate tunnel. Looking up the rock test for coal mines located in this district [24], the relative permittivity of the rock was around 10-15. In this simulation, it was assumed that $K1 = K2 = 12$.

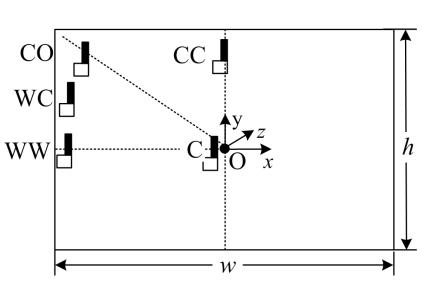

Equivalent Coordinates of Antennas

The fixed end	
C	(-0.28, 0, 0)
CC	(-0.08, 1.43, 0)
CO	(-2.15, 1.42, 0)
WC	(-2.30, 0.95, 0)
WW	(-2.31, 0.14, 0)
The mobile end	
C	(0, 0.06, z)

w=5.10m, h=3.43m,
$K1$=$K2$=12

FIGURE 6. Simulation parameters of the equivalently surrogated rectangular tunnel with antenna positions.

Table 3 presents the calculated mean error and error SD between the theoretical and measured results. The error was within the acceptable range. The reasons for the inaccuracies were as follows.

1) The parameters of the surrogate rectangular tunnel were not necessarily the best values, as their optimization was beyond the purpose of this study.
2) In the arched tunnel, the EM wave excited by the antenna at different positions presented different degrees of depolarization [16], [18]. However, no depolarization was assumed in the theory of propagation for the rectangular tunnel.
3) The actual EM environment was not ideal. Scatters, such as rails, cables, and pipes, were present in the gallery. Deformation was observed on the wall.

Using max $\left(w^2/\lambda, h^2/\lambda\right)$ [8], the break point of the near and far-field regions in the tunnel was about 37.51 m away

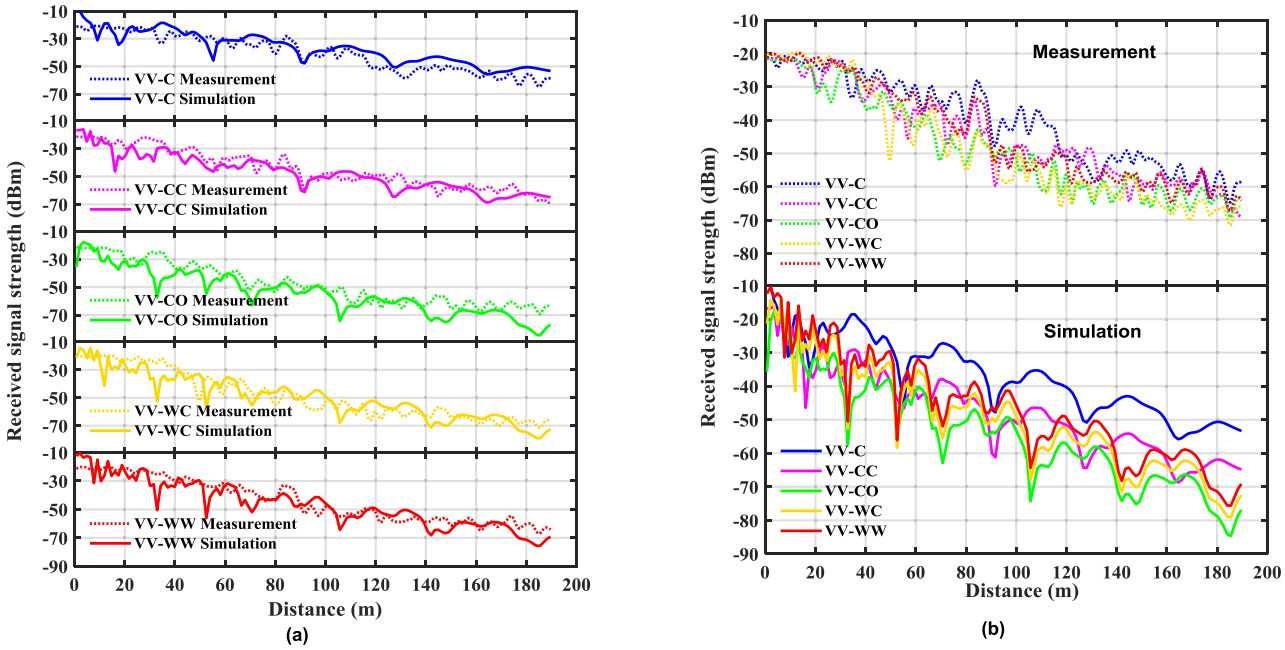

FIGURE 7. Distance-dependent signal power in underground mine when antennas are vertically polarized. (a) Results for each receiving location. (b) Results for location differential.

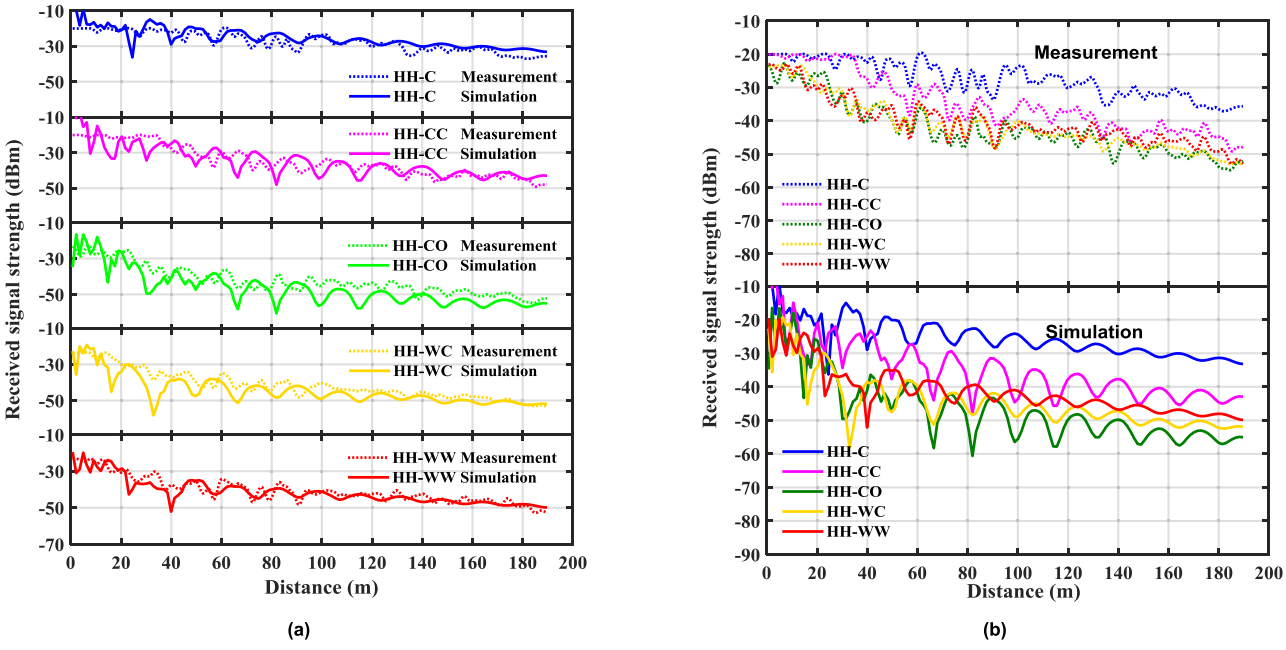

FIGURE 8. Distance-dependent signal power in underground mine when antennas are horizontally polarized. (a) Results for each receiving location. (b) Results for location differential.

from the transmitting antenna. The field coverage in these two regions was compared in Tables 4, 5, and 6.

A. COMPARISON OF FIELD IN NEAR-FIELD REGION

1) LOCATION DIFFERENTIAL

Table 4 shows the differences in the field power for different antenna positions. In the near-field region, both the measured and theoretical comparisons showed that mounting the vertically polarized antenna on the sidewalls could produce greater field strength; while mounting horizontally polarized antenna on the ceiling could result in a stronger field. This was consistent with the results of the measurements conducted at ranges of 32 m in a tunnel in [7]. Besides, both the polarized antennas nearly had the weakest signal strength at the CO position and the strongest strength at the C position. These results were consistent with the prediction in Section II.

TABLE 3. Comparison of field power between measurement and simulation.

Location differential	Mean error (dBm)	Error standard deviation (dBm)
Vertical polarization		
C_VV	3.49	5.72
CC_VV	−2.88	6.08
CO_VV	−6.11	7.27
WC_VV	−1.24	8.20
WW_VV	−2.31	6.66
Horizontal polarization		
C_HH	1.92	3.89
CC_HH	−0.29	5.58
CO_HH	−4.32	5.38
WC_HH	−3.08	4.50
WW_HH	−1.09	3.82

TABLE 4. Average signal strength (in dBm) received at different positions.

Location	Near-field region		Far-field region	
	Experiment	Simulation	Experiment	Simulation
Vertical polarization				
C_VV	−23.67	−21.83	−44.57	−40.67
CC_VV	−24.31	−29.48	−49.72	−52.04
CO_VV	−25.65	−33.03	−53.74	−59.54
WC_VV	−22.04	−28.05	−55.07	−55.12
WW_VV	−22.47	−24.60	−49.46	−51.81
Horizontal polarization				
C_HH	−20.82	−18.47	−29.07	−27.25
CC_HH	−21.08	−23.41	−38.31	−38.09
CO_HH	−29.28	−32.73	−45.66	−50.19
WC_HH	−28.78	−34.37	−44.53	−46.99
WW_HH	−29.24	−31.56	−43.20	−43.99

2) POLARIZATION DIFFERENTIAL

Table 5 shows the differences in the field power for different antenna polarizations. As can be seen, for WC and WW locations, vertically polarized links presented stronger average path power in the near-field region, while for the position of CC point, horizontally polarized links exhibited stronger average path power. This result was also consistent with the previous study in [7]. The reasons have been interpreted in Section II. It also could be explained from the view of the ray theory discussed in [7].

TABLE 5. Average difference in signal strength (in dBm) for horizontally and vertically polarized waves.

Polarization	Near-field region		Far-field region	
	Experiment	Simulation	Experiment	Simulation
VV-to-HH_C	−2.85	−3.09	−15.50	−13.42
VV-to-HH_CC	−3.23	−6.43	−11.41	−13.95
VV-to-HH_CO	3.63	−0.3	−8.08	−9.35
VV-to-HH_WC	6.74	6.32	−10.54	−8.13
VV-to-H_WW	6.77	6.96	−6.26	−7.82

Table 6 compares the average path strength for the better deployment scenarios. Generally speaking, the differences among these deployments in the near-field region were rather small. The measured differences were no more than 1.5 dBm, and the theoretical differences were no more than 5 dBm. The slight differences were due to the fact that multiple modes participating in the propagation in this region.

TABLE 6. average difference in signal strength (in dBm) for three preferred deployment methods.

Deployment differential	Near-field region		Far-field region	
	Experiment	Simulation	Experiment	Experiment
VV at WW-to-HH at CC	−1.39	−1.19	−11.15	−13.72
VV at WC-to-HH at CC	−0.96	−4.64	−16.76	−17.03

B. COMPARISON OF FIELD IN FAR-FIELD REGION

1) LOCATION DIFFERENTIAL

As shown in Table 4, both horizontally and vertically polarized antennas had the weakest signal strength at the CO position and the strongest strength at the C position in the far-field region, and similar results could be obtained for the near-field region. However, comparisons of other positions demonstrated some different characteristics. Mounting the antenna at the CC position and the WW position obtained the stronger signal power, whereas mounting the antenna at the WC position obtained much weaker signal power. These were consistent with the prediction in Section II.

2) POLARIZATION DIFFERENTIAL

As shown in Tables 5, in the far-field region, both the measured and the theoretical results showed that for all observation locations, the signal coverage of the horizontally polarized links was much stronger than that of the vertically polarized links. As described in Section II, the reasons was that the significant mode in the far-field region was the (1, 1) mode for both horizontal and vertical polarizations, and the coupling efficiency of the (1, 1) mode for these two polarizations was nearly the same, but horizontal polarization could get less propagation loss.

C. EFFECT OF UNDERGROUND INFRASTRUCTURE

The industrial EM noise generated by the coal mine infrastructure in different regions has a great influence on the power fluctuation of the covered field. The applicability of the theoretical deployment in real mines is limited. This study mainly focused on the effect of the cables that existed in all tunnels.

For the grid experiments, the position of C was furthest away from all facilities. The position of WW was relatively far away. The positions of CO, CC and WC were near the communication cables, the overhead cable driving narrow-gauge vehicle, and the power cables for mining machines, respectively. Considering the test data of each group for 3 min as a unit, the deviation value from the mean received power was calculated. After measurements over several days, the probability of deviation from the mean measured signal in a small time interval is shown in Fig.9.

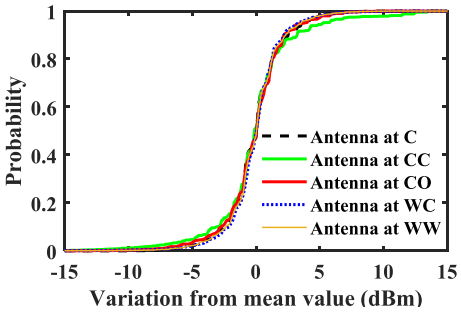

FIGURE 9. Deviation from the mean measured signal in a small time interval (3 min) due to EM interference.

The results showed that the field fluctuation in a small time interval was the most severe when the antenna was at the CC position. The maximum deviation could be 12 dBm from the average power. The reason was that the field at the CC position was affected by the unstable power load of the cable due to intermittent operation of the locomotive. For other locations, the probability of the field deviation was much smaller, because the power load of nearby cables varied less due to the continuous and relatively stable operation of the mining equipment and communication equipment. In addition, their probabilities of the field deviation were rather similar because of the spatial constraints of the tunnel. Hence, it was not necessary to consider the influence of the power cables and communication cables when arranging the antenna positions.

V. CONCLUSION

In this study, the optimal antenna polarization and position were proposed to enhance the field coverage for wireless communications in underground coal mines. The optimization was based on the multimodal approach, which provided the order of the significant modes for the field propagation and the coupling efficiency of the antenna to the modes. The analyzed results showed that:

1) In the near-field region of the source, the effect of antenna polarization on the filed fading depended upon antenna position.
   - For vertical polarization, the modes with n = 1, 2, and 3 played a significant role in the signal propagation. Installing vertically polarized antenna on the sidewalls could effectively excite them and present stronger field power.
   - For horizontal polarization, the modes with m = 1, 2, and 3 were significant, and the optimal mounting location was the ceiling.
2) In the far-field region, antenna polarization alone had a deterministic effect on the filed fading.
   - Only horizontal polarization could provide lower field attenuation, and the optimal mounting location of the antenna was the center of the ceiling or that of the sidewalls.

A grid-based test system was designed, and a series of measurements were conducted inside an underground coal mine tunnel for verification. The measured results had a good agreement with the theoretical ones, which verified that the proposed deployment strategy had a good performance and potential applications for coal mines.

REFERENCES

[1] J. Wang, Y. Guo, Y. Jia, Y. Zhang, and M. Li, "Modeling and application of the underground emergency hedging system based on Internet of Things technology," *IEEE Access*, vol. 7, pp. 63321–63335, 2019.
[2] X. Liu, X. Yin, and G. Zheng, "Experimental investigation of millimeter-wave MIMO channel characteristics in tunnel," *IEEE Access*, vol. 7, pp. 108395–108399, 2019.
[3] A. Chehri, G. Jeon, and B. Choi, "Link-quality measurement and reporting in wireless sensor networks," *Sensors*, vol. 13, no. 3, pp. 3066–3076, 2013.
[4] Y. Huo, Z. Xu, H.-D. Zheng, and X. Zhou, "Effect of antenna on propagation characteristics of electromagnetic waves in tunnel environments," in *Proc. Asia–Pacific Conf. Postgraduate Res. Microelectron. Electron. (PrimeAsia)*, Shanghai, China, Nov. 2009, pp. 268–271.
[5] J. Wang, Y. Huang, and D. Li, "Research on the field coverage generated by antennas in confined space," in *Proc. 3rd Asia–Pacific Conf. Antennas Propag.*, Harbin, China, Jul. 2014, pp. 775–778.
[6] D. Li and J. Wang, "Effect of antenna parameters on the field coverage in tunnel environments," *Int. J. Antennas Propag.*, vol. 2016, pp. 1–10, 2016.
[7] S. Bashir, "Effect of antenna position and polarization on UWB propagation channel in underground mines and tunnels," *IEEE Trans. Antennas Propag.*, vol. 62, no. 9, pp. 4771–4779, Sep. 2014.
[8] Y. P. Zhang, "Novel model for propagation loss prediction in tunnels," *IEEE Trans. Veh. Technol.*, vol. 52, no. 5, pp. 1308–1314, Sep. 2003.
[9] M. A. Moridi, Y. Kawamura, M. Sharifzadeh, E. K. Chanda, and H. Jang, "An investigation of underground monitoring and communication system based on radio waves attenuation using ZigBee," *Tunnelling Underground Space Technol.*, vol. 43, pp. 362–369, Jul. 2014.
[10] C. Zhou, T. Plass, R. Jacksha, and J. A. Waynert, "RF propagation in mines and tunnels: Extensive measurements for vertically, horizontally, and cross-polarized signals in mines and tunnels.," *IEEE Antennas Propag. Mag.*, vol. 57, no. 4, pp. 88–102, Aug. 2015.
[11] A. Ranjan, H. B. Sahu, and P. Misra, "Modeling and measurements for wireless communication networks in underground mine environments," *Measurement*, vol. 149, Jan. 2020, Art. no. 106980.
[12] A. Ranjan, H. B. Sahu, and P. Misra, "MineSense: Sensing the radio signal behavior in metal and non-metal underground mines," *Wireless Netw.*, vol. 25, no. 6, pp. 3643–3655, Aug. 2019.
[13] K. Guan, Z. Zhong, B. Ai, R. He, B. Chen, Y. Li, and C. Briso-Rodriguez, "Complete propagation model structure inside tunnels," *Prog. Electromagn. Res.*, vol. 141, pp. 711–726, 2013.
[14] Z. Sun and I. Akyildiz, "Channel modeling and analysis for wireless networks in underground mines and road tunnels," *IEEE Trans. Commun.*, vol. 58, no. 6, pp. 1758–1768, Jun. 2010.
[15] F. Fuschini and G. Falciasecca, "A mixed rays—Modes approach to the propagation in real road and railway tunnels," *IEEE Trans. Antennas Propag.*, vol. 60, no. 2, pp. 1095–1105, Feb. 2012.
[16] X. Zhang and C. D. Sarris, "Vector parabolic equation-based derivation of rectangular waveguide surrogate models of arched tunnels," *IEEE Trans. Antennas Propag.*, vol. 66, no. 3, pp. 1392–1403, Mar. 2018.
[17] S. F. Mahmoud, "Wireless transmission in tunnels with non-circular cross section," *IEEE Trans. Antennas Propag.*, vol. 58, no. 2, pp. 613–616, Feb. 2010.
[18] J. M. Molina-Garcia-Pardo, M. Lienard, A. Nasr, and P. Degauque, "On the possibility of interpreting field variations and polarization in arched tunnels using a model for propagation in rectangular or circular tunnels," *IEEE Trans. Antennas Propag.*, vol. 56, no. 4, pp. 1206–1211, Apr. 2008.
[19] Y. Yamaguchi, T. Abe, T. Sekiguchi, and J. Chiba, "Attenuation constants of UHF radio waves in arched tunnels (Short Paper)," *IEEE Trans. Microw. Theory Techn.*, vol. MTT-33, no. 8, pp. 714–718, Aug. 1985.
[20] K. D. Laakmann and W. H. Steier, "Waveguides: Characteristic modes of hollow rectangular dielectric waveguides," *Appl. Opt.*, vol. 15, no. 5, pp. 1334–1340, May 1976.
[21] A. Emslie, R. Lagace, and P. Strong, "Theory of the propagation of UHF radio waves in coal mine tunnels," *IEEE Trans. Antennas Propag.*, vol. 23, no. 2, pp. 192–205, Mar. 1975.

[22] B. Sturani and A. Coraiola, "Using a pair of phased antennas to improve UHF reception/transmission in tunnels," *IEEE Antennas Propag. Mag.*, vol. 42, no. 5, pp. 40–47, Oct. 2000.
[23] A. R. Silva and M. C. Vuran, "Development of a testbed for wireless underground sensor networks," *EURASIP J. Wireless Commun. Netw.*, vol. 2010, no. 1, pp. 1–14, Dec. 2010.
[24] G. Z. Yang, "Research on coal-rock interface recognition technology based on ground penetrating radar," M.S. thesis, China Univ. Mining Technol., Xuzhou, China, May 2019, pp. 15–26.

YU HUO (Member, IEEE) was born in Wushan, China, in 1983. She received the Ph.D. degree in communication and information system from the China University of Mining and Technology (CUMT), Xuzhou, China, in 2013.

She is currently a Research Assistant with the National Joint Engineering Laboratory of Internet Applied Technology of Mines, CUMT. Her main fields of interest are antenna systems and propagation models, wireless underground networks, and emergency rescue communication.

LEI ZHAO (Senior Member, IEEE) received the B.S. degree in mathematics from Jiangsu Normal University, China, 1997, and the M.S. degree in computational mathematics and the Ph.D. degree in electromagnetic fields and microwave technology from Southeast University, Nanjing, China, in 2004 and 2007, respectively.

From September 2009 to December 2018, he worked in Jiangsu Normal University, Xuzhou, China. From August 2007 to August 2009, he worked in the Department of Electronic Engineering, The Chinese University of Hong Kong as a Research Associate. From February 2011 to April 2011, he worked in the Department of Electrical and Computer Engineering, National University of Singapore as a Research Fellow. From September 2016 to September 2017, he worked in the Department of Electrical and Computer Engineering, University of Illinois at Urbana–Champaign, USA as a Visiting Scholar. He joined the China University of Mining and Technology, Xuzhou, China, in 2019, where he is currently the Full Professor. He has authored and coauthored more than 60 refereed journal and conference papers. His current research interests include spoof surface plasmon polaritons theory and its applications, antennas design and its applications, computational electromagnetics, and electromagnetic radiation to human's body.

Dr. Zhao serves as an Associate Editor for IEEE Access, an Associate Editor-in-Chief for *ACES* Journal and a Reviewer for multiple journals and conferences including the IEEE Transactions on Microwave Theory and Techniques, the IEEE Transactions on Antennas and Propagation, IEEE Access, the IEEE Antennas and Wireless Propagation Letters, *ACES* Journal, and other primary electromagnetics and microwave related journals.

QINGSONG HU received the B.S. degree in medical imaging and the M.S. and Ph.D. degrees in communication and information system from the China University of Mining and Technology (CUMT), Xuzhou, China, in 2001, 2004, and 2011, respectively.

He is currently an Associate Professor with CUMT. His main research interests include the mine Internet of Things, mobile object localization, and emergency communications.

ENJIE DING received the B.S., M.S., and Ph.D. degrees in control theory and control engineering from the China University of Mining and Technology (CUMT), Xuzhou, China.

He is currently the Director and Professor of the National Joint Engineering Laboratory of Internet Applied Technology of Mines, CUMT. His main research interests include signal processing, wireless communications, wireless sensor networks, and the Internet of Things in coal mines.

XIAOHU ZHAO was born in Xuzhou, China, in 1976. He received the Ph.D. degree in control theory and control engineering from the China University of Mining and Technology (CUMT), Xuzhou, China, in 2007.

He is currently the Deputy Director and Professor of the National Joint Engineering Laboratory of Internet Applied Technology of Mines, CUMT. His main research interests include the mine Internet of Things, mine communications, monitoring and control, computer networks, and intelligent computing.

ZHI SUN (Member, IEEE) received the B.S. degree in telecommunication engineering from the Beijing University of Posts and Telecommunications (BUPT), Beijing, China, in 2004, the M.S. degree in electronic engineering from Tsinghua University, Beijing, China, in 2007, and the Ph.D. degree in electrical and computer engineering from the Georgia Institute of Technology, Atlanta, USA, in 2011.

He was a Postdoctoral Fellow with the Georgia Institute of Technology, Atlanta, USA, from 2011 to 2012. He joined the Department of Electrical Engineering, University at Buffalo, State University of New York, Buffalo, NY, USA, as an Assistant Professor in 2012, where he is currently an Associate Professor. His research interests include wireless communication and networking in extreme environments, metamaterial enhanced communication and security, physical-layer security, wireless intrabody networks, wireless underground networks, wireless underwater networks, and cyber physical systems.

Prof. Sun was a recipient of the NSF CAREER Award, in 2017, the UB Exceptional Scholar-Young Investigator Award, in 2017, the Best Demo Award in IEEE INFOCOM 2017, the Best Paper Award in IEEE GLOBECOM, in 2010, the BWN Researcher of the Year Award at the Georgia Institute of Technology, in 2009, and the Outstanding Graduate Award at Tsinghua University, in 2007. He currently serves as an Editor for the IEEE Transactions on Wireless Communications and *Computer Networks* Journal (Elsevier).